Dynamic Restoration of Active Distribution Networks by Coordinated Repair Crew Dispatch and Cold Load Pickup

Dynamic Restoration of Active Distribution Networks by Coordinated Repair Crew Dispatch and Cold Load Pickup

Kaiyuan Pang, *Graduate student Member*, *IEEE*, Chongyu Wang, *Member*, *IEEE*, Nikos D. Hatziargyriou, *Life Fellow*, *IEEE*, Fushuan Wen, *Fellow*, *IEEE*

Abstract—This paper presents a dynamic restoration strategy for active distribution networks (ADNs) by coordinating repair crew dispatch and frequency-constrained cold load pickup. To incorporate the stochastic repair time, the repair crew dispatch is formulated as "event-driven" with the implementation of model predictive control (MPC). The stochastic repair time is estimated, convexified, and updated dynamically with each MPC execution. The finish of a repair task triggers the subsequent cold load pickup model, where the frequency dynamics are computed and linearly constrained with the help of a uniform frequency response model for low-inertia systems. Next, a co-optimization framework of the two models is developed to coordinate the repair crew dispatch and cold load pickup under a unified time scale. Numerical results on a modified IEEE 33-node test feeder and a real-world 136-node distribution system have verified the effectiveness of the proposed model.

***Index Terms*—Active distribution network, dynamic restoration, repair crew dispatch, cold load pickup, frequency dynamics.**

NOMENCLATURE

Indices and Sets

$i, j, m, n \in \mathcal{N}$	Indices and set of nodes.
$(i,j), (m,n) \in \mathcal{E}$	Indices and set of branches.
$\mathcal{E}_{\mathrm{F}}, \mathcal{E}_{\mathrm{O}}, \mathcal{E}_{\mathrm{N}} \subseteq \mathcal{E}$	Set of faulted branches, outage branches without faults, and operating branches.
$\mathcal{E}_{ij} \subseteq \mathcal{E}$	Set of branches adjacent to branch(i,j).
$\mathrm{c} \in \mathcal{C}$	Index and set of repair crews.
$k, l \in \mathcal{K}$	Indices and set of recovery operations.
$g \in \mathcal{G}$	Index and set of synchronous generators.
$d \in \mathcal{D}$	Index and set of droop-controlled DGs.
$v \in \mathcal{V}$	Index and set of VSM-controlled DGs.

Parameters

R_{ij}, X_{ij}	Resistance and reactance of branch (i,j).
$V_{\min}, V_{\max}$	Minimum and maximum voltage magnitude.
$F_{ij,\max}$	Maximum apparent power allowed to flow on branch (i,j).
$P^{\mathrm{G}}_{i,\min}, P^{\mathrm{G}}_{i,\max}$	Minimum and maximum active power generation at node i.
S^{G}_i	Rated capacity of the generator at node i.
$P^{\mathrm{L}}_i, Q^{\mathrm{L}}_i$	Rated active and reactive power demands of the load at node i.
$TR^{\mathrm{avg}}_{c,mn}$, $TR^{\mathrm{var}}_{c,mn}$	Mean and variance of the repair time required by repair crew c to fix branch (m,n) (the rough approximation).
$TA^{\mathrm{avg}}_{c,mn}$, $TA^{\mathrm{var}}_{c,mn}$,	Mean and variance of the repair time required by repair crew c to fix branch (m,n) (the more accurate approximation).
$TA^{-}_{c,mn}$, $TA^{+}_{c,mn}$	Pessimistic and optimistic estimation of the repair time required by repair crew c to fix branch (m,n) (the more accurate approximation).
$T^{\mathrm{tr}}_{ij,mn}, T^{\mathrm{tr}}_{0,mn}$	Transportation time from branch (i,j) and repair station to (m,n).
λ_i	Weighted coefficient of load at node i.
T_{end}	User-defined end time of the restoration process.
ε	User-defined probability level.
$P^{\mathrm{T}}_i, P^{\mathrm{S}}_i$	Magnitude of the transient and steady-state plateaus of the CLPU curve of node i.
T_1	Duration of the transient process of CLPU.
ρ	The ratio of the steady-state plateau to the transient plateau in the CLPU curve.
M, D	Aggregate inertia and damping constants of the energized part of the ADN.
$\mathrm{RoCoF}_{\max}$	Maximum RoCoF allowed.
$\Delta f^{\mathrm{ndr}}_{\max}$	Allowed frequency nadir.
$\Delta f^{\mathrm{ss}}_{\max}$	Maximum steady-state frequency deviation.
$x_{i,\infty}, y_{ij,\infty}$, $x^{\mathrm{L}}_{i,\infty}$	Energization statuses of nodes, branches, and loads in the restored ADN.

Decision Variables of the Repair Crew Dispatch Model

$z_{c,mn,k}$	Binary repair decision of faulted branch (m,n) made by repair crew c in the k^{th} recovery operation.
t_{mn}	Restoration time of faulted branch (m,n).
t^{F}_k	Finishing time of the k^{th} recovery operation.
$u_{mn,k}$	Binary status of faulted branch (m,n).
$x_{i,k}, y_{ij,k}$	Binary status of node *i* and branch (i,j).

This work was supported by the National Natural Science Foundation of China under Grant U1910216.

K. Pang, C. Wang, and F. Wen are all with the College of Electrical Engineering, Zhejiang University, Hangzhou 310027, China (e-mail: kaiyuan.pang@zju.edu.cn; chongyu.wang@outlook.com; fushuan.wen@gmail.com). K. Pang is also with the National Technical University of Athens, Athens 15773, Greece, as a visiting Ph.D. student. C. Wang is also with the Department of Electrical Engineering, The Hong Kong Polytechnic University, Kowloon, Hong Kong S.A.R., China. F. Wen is also with Hainan Institute, Zhejiang University, Sanya 572024, China.

N. D. Hatziargyriou is with the National Technical University of Athens, Athens 15773, Greece and a part-time Professor at the University of Vaasa, Wolffintie 32, Vaasa 65200, Finland (e-mail: nh@power.ece.ntua.gr).

$x^{\mathrm{L}}_{i,k}$	Binary status of the load at node i.
$p_{ij,k}, q_{ij,k}$	Active and reactive power flows on branch (i,j).
$p^{\mathrm{G}}_{i,k}, q^{\mathrm{G}}_{i,k}$	Active and reactive power generation at node i.
$p^{\mathrm{L}}_{i,k}, q^{\mathrm{L}}_{i,k}$	Active and reactive load demand at node i.
$v_{i,k}$	Squared value of voltage magnitude of node i.
$t_{c,mn,k}$	Required repair time if faulted branch(m,n) is repaired by repair crew c in the k^{th} recovery operation.
$w_{ij,mn}$	Binary variable denoting that branch (m,n) is fixed following branch (i,j) by the same repair crew.
$w_{0,mn}$	Binary variable denoting that branch (m,n) is first fixed.

Decision Variables of the Sequential Cold Load Pickup Model

The definition of the following variables is the same as that of the repair crew dispatch model with subscript k discarded.

$x_i, y_{ij}, x^{\mathrm{L}}_i$	Topology-related variables.
$p_{ij}, q_{ij}, p^{\mathrm{G}}_i, q^{\mathrm{G}}_i, p^{\mathrm{L}}_i, q^{\mathrm{L}}_i, v_i$	Power flow-related variables.

I. Introduction

FAST and efficient restoration is crucial for enhancing distribution system resilience. High resilience has become an increasingly challenging problem for *Active Distribution Networks* (ADNs) that require well-designed control schemes for active lines and *Distributed Energy Resources* (DER) [1]. The restoration process, involving comprehensive coordination of repair crew dispatch, switch operations, and load pickup meeting the transient and steady-state security constraints, is known as one of the most complicated power system optimization problems [2].

In order to simplify the problem, the restoration process is assumed to be divided into multiple steps with a fixed duration. This extensively adopted assumption lies in the backbone of modeling the repair crew dispatch in ADNs. Based on the modeling techniques of the *Vehicle Routing Problem* (VRP), the repair crew dispatch is formulated as a *Mixed-Integer Linear Programming* (MILP) problem in [3], considering the interdependence between crew traveling and repairing. References [4] and [5] further develop the role of a repair crew into operating manual switches and clearing faults, which are co-optimized to provide a pragmatic crew dispatch scheme. The models developed in [3-5] are complicated and time-consuming to solve, so preliminary processes, including clustering loads into a node cell and pre-assigning faults to a repair station/depot, are used to ease the computational burden [6]. The discussed repair crew dispatch models [3-6] rely on a binary variable $z_{c,m,n}$, indicating whether crew c travels from fault m to fault n. Then the energization statuses of faulted components are determined and assigned to a pre-defined time series, based on crews' travel time, repair time, and the routing path $z_{c,m,n}$.

Another modeling method for repair crew dispatch directly associates the repair operation with specific time steps, using a binary variable $z_{c,m,t}$ to denote whether crew c is repairing fault m at time step t. Typically, the travel time and repair time should be provided as deterministic inputs, for imposing restrictions on adjacent time steps of $z_{c,m,t}$ [7]. This type of modeling makes it convenient to coordinate repair crew dispatch with subsequent system reconfiguration and scheduling problems [8-9]. On this basis, simpler and efficient models are developed. In [10] and [11], the number of repair crews is modeled as restoration resources to restrict the number of faults under clearance at a time step. As a result, $z_{c,m,t}$ is simplified as $z_{m,t}$, denoting whether fault m is being repaired at time step t. In [12], the restoration time of a fault is estimated using the upper bounds of the travel time and repair time. Then this restoration time is imposed on $z_{m,t}$ to guarantee that enough and consecutive time steps be spent on repairing the fault.

TABLE I Comparisons of repair crew dispatch models

Models	Characteristics	Pros and cons*
VRP-based models [3-6]	1. Decision variable $z_{c,m,n}$ 2. Detailed modeling of repair crew routing 3. Restoration time is obtained by summing up the travel time and repair time in a routing path	[p] Benchmark models for comparison and improvement [c] Need additional constraints to couple $z_{c,m,n}$ and components' energization statuses [c] High complexity: a pre-assignment process is required
Multi-time-step models [7-12]	1. Decision variable $z_{c,m,t}/z_{m,t}$ 2. Repair operations are associated directly with time steps 3. Deterministic travel time and repair time	[p] Easy to integrate subsequent system reconfiguration and scheduling problems [p] Able to be simplified as needed [c] Inaccurate restoration time by large duration between adjacent time steps [c] Unable to incorporate stochastic travel and repair time
Stochastic models [13, 14]	1. Based on the VRP model [3] 2. Truncated normal distribution and (truncated) lognormal distribution are assumed for travel time and repair time 3. Monte Carlo-based sample generation	[p] First attempts to tackle stochastic travel and repair time [c] Hard to obtain the probability distribution [c] Significantly increased complexity due to numerous samples
Event-driven model [15]	1. Decision variable $z^{k}_{c,m,n}$, where k denotes a repair event 2. The pre-defined time series is discarded	[p] Restoration time is more accurate [c] Over-complicated

* The pros and cons are indicated by [p] and [c] in this column

The characteristics of the aforementioned two types of repair crew dispatch models are summarized as VRP-based models [3-6] and multi-time-step models [7-12] in TABLE I. Following these existing models, recent research efforts highlight the necessity to address stochastic travel and repair time [13, 14] as well as event-driven repair crew dispatch [15]. These recent improvements are discussed as follows.

1) Stochastic modeling of repair crew dispatch: This modeling technique is important as crew traveling and repairing processes are highly stochastic in the real world; if neglected, the resulting solution could lead to suboptimality. In the worst case, it can provide prohibitive operations, e.g., energizing a large load in a heavily loaded subsystem before *Distributed Generators* (DGs) are restored. This is because by deterministic modeling, the DGs are always assumed to be restored earlier than the large load, while an opposite situation may occur due to the stochasticity of the repair process. To overcome this difficulty, stochastic optimization techniques are employed, and the repair time is assumed to follow a lognormal distribution [13] or truncated lognormal distribution [14]. The Monte Carlo

sampling method is then adopted to convey the stochasticity to numerous deterministic scenarios. In other words, the stochastic repair time is addressed by a deterministic optimization problem with numerous scenarios. However, the large number of scenarios can lead to intractability of the problem. In this regard, a novel repair crew dispatch model is entailed to address the stochastic repair process with reduced complexity

2) Event-driven modeling of repair crew dispatch: As noted, the application of the repair crew dispatch models in [3-12] requires a pre-defined time series with a fixed duration (e.g., $[t_1, t_2, \dots, t_n]$ and $\Delta t = t_2 - t_1 = \cdots = t_n - t_{n-1} = 30$ min). Although a smaller duration (e.g., $\Delta t = 5$ min) provides a more accurate repair crew dispatch scheme, it drastically increases the complexity of the restoration model that normally extends to hundreds of minutes. On the other hand, defining a larger duration (e.g., $\Delta t = 60$ min) could lead to unpractical solutions. For example, if a repair crew clears a fault at the 61st min, the multi-time-step models only allow the newly restored component to be energized in the next time step, i.e., the 120th min, prolonging the restoration process by 59 min. To overcome this difficulty, an event-driven repair crew dispatch model is proposed in [15] to avoid the pre-defined time series, and the clearance time of faults will be the "exact" instant when they are removed, e.g., the 59th or 61st min. However, the binary variable $z_{c,m,n}$ defined in [3] are duplicated once for every repair event as $z^k_{c,m,n}$ (k indicates a repair event) in [15], overcomplicating the mathematical model. Hence, modeling repair crew dispatch in an event-driven manner without significantly affecting the problem complexity is another crucial task.

Given these two recent improvements and their limitations, a novel modeling method of repair crew dispatch is entailed to consolidate and incorporate the stochastic and event-driven characteristics in one model. Moreover, this model should be highly tractable, as a fundamental requirement is that the ADN restoration problem should be solved in a relatively short time. In this regard, considering the restoration process dynamically permits more efficient dispatch of repair crews, by looking ahead only a few future operations. In this way, the model complexity can be significantly reduced. The well-established *Model Predictive Control* (MPC), due to its cyclic "prediction-solution-implementation" characteristic, is ideally suited for the event-driven repair crew dispatch. Moreover, compared to sampling numerous scenarios, convex approximation of the stochastic repair time contributes to a more efficient optimization model. Therefore, it is challenging and crucial to design a new repair crew dispatch model to incorporate these advanced and promising modeling techniques.

Another major factor requiring a dynamic approach to ADN restoration is the *Cold Load Pickup* (CLPU) effect, which results in a drastic increase in load demand due to the transient inrush current and loss of diversity [16]. In ADNs embedded with numerous inverter-interfaced DGs that generally do not contribute to inertia provision, the system frequency subject to CLPU could drop dramatically, causing undesirable protection operation to trip loads and DGs. Several research efforts have formulated the CLPU effect by historical data fitting. The report [16] provides some essential data and analysis for modeling the CLPU, such as the lasting time, transient peak, and impact factors of the peak power demand. On this basis, a simple model considering only the transient peak is proposed in [17]. For higher accuracy, the CLPU demand is formulated as an exponentially decreasing curve [18]. However, the data required for modeling the exponential curve is only available after the end of the CLPU effect. Hence, it is suggested in [19] to use a more general model considering the peak value and lasting time of the CLPU effect. Even with a proper CLPU model used, the calculation of the frequency dynamics subject to CLPU remains demanding. The dynamic frequency profile is typically computed by electromechanical transient simulation using detailed control parameters. For example, a second-level simulation model is proposed in [20] to obtain the transient frequency nadir after load pickup, which is then fed back to the first-level optimization model. Alternatively, to formulate the frequency dynamics mathematically, reference [21] provides a uniform frequency response model for low-inertia power systems considering both the traditional governor control and converter-based control. With applications to the unit commitment problem, the accuracy of this model has been validated with simulation data [22]. Typically, the load pickup power is formulated as a constant input for the uniform frequency response model [21]. Then the system frequency can be obtained by solving the swing equation. However, the CLPU demand is time-dependent, involving a transient peak and a gradually decreasing steady-state curve. This makes the calculation of frequency dynamics challenging. In this regard, it is of practical significance to develop a transient frequency-constrained CLPU model, as the fast-changing frequency is a primary cause of instability in low-inertia ADNs [23]. To achieve this, new modeling techniques of the CLPU effect and their applications in calculating frequency dynamics remain to be investigated.

Given the background above, this paper contributes to dynamic ADN restoration by coordinating two improved models, the event-driven *Repair Crew Dispatch* (RCD) model and the transient frequency-constrained *Sequential Cold Load Pickup* (SCLP) model. The main contributions are detailed below:

1) A novel event-driven RCD model with reduced complexity and improved capability is formulated to address stochastic repair time. Compared to the binary variable $z^k_{c,m,n}$ used in the event-driven model [15], the proposed event-driven RCD model requires only a 3-dimensional binary variable $z_{c,m,k}$. Besides, the stochastic repair time is addressed by convex approximation instead of scenario generation used in [13, 14], avoiding to overcomplicate the model. A dynamic update scheme is also designed to evaluate the stochastic repair time dynamically and more accurately, based on different timings of the RCD process.

2) A frequency-constrained SCLP model is developed, where the transient *Rate of Change of Frequency* (RoCoF), frequency nadir, and steady-state frequency can be imposed as convex constraints. To achieve this, the peak demand model [17] of the CLPU effect is improved as a step function considering the transition between the transient and steady-state demands. Then the expressions of the three frequency indicators are derived with mathematical details, using the improved CLPU

model as the input.

3) A MPC-based co-optimization framework is designed for the proposed RCD and SCLP models to facilitate dynamic and real-time ADN restoration. The MPC-based framework is able to respond to real-time repair events, including the arrival of repair crews and the completion of fault clearance, by recursively updating system conditions and co-optimizing the RCD and SCLP models. Under this framework, the dispatch of repair crews and implementation of load pickups are coordinated to restore de-energized loads quickly and securely.

The remainder of this paper is organized as follows. Section II discusses the coordination between the RCD and SCLP models. Sections III and IV formulate the event-driven RCD and frequency-constrained SCLP models, respectively. Section V presents the solution methodology of these two models. Numerical results are given in Section VI. Section VII concludes the paper.

II. Coordination between RCD and SCLP

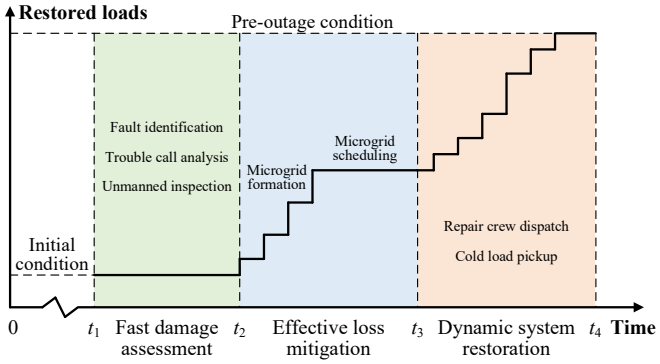

Fig. 1 Restoration of an ADN subject to catastrophic events.

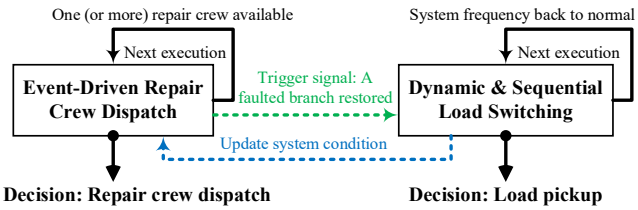

Fig. 2 Co-optimization framework of the proposed RCD and SCLP models.

To highlight the effectiveness of the proposed dynamic ADN restoration strategy, this paper focuses on a worst case, i.e., the ADN is suffering simultaneous substation disconnection and internal faults. Fig. 1 depicts the typical stages of restoring such a faulted ADN. The fast damage assessment aims to identify trouble spots, evaluate the extent of damages, and estimate required restoration resources [24]. Useful information can be obtained from advanced fault diagnosis and identification algorithms [25], consumers' trouble calls, and unmanned inspection systems [26]. Next, effective loss mitigation is conducted to provide emergency support to critical loads, utilizing available and controllable DGs. In this stage, restorative operations are executed to separate the faulted system into one or multiple microgrids that can function sustainably [27]. Lastly, in the dynamic restoration stage, the formed microgrids are extended and interconnected, and the faulted system returns to the normal operating state gradually. The practical and significant issue during this stage is to coordinate the repair crew dispatch and cold load pickup.

Targeting at the dynamic system restoration stage, the proposed strategy is implemented at time instant t_3, when the fast damage assessment and effective loss mitigation stages have been completed. Hence, fault knowledge (e.g., locations and types of faults) and components' energization statuses are considered as deterministic input parameters, and DGs' black-start process is considered finished.

The proposed dynamic ADN restoration strategy consists of two stages: an event-driven RCD model and a frequency-constrained SCLP model. Fig. 2 illustrates the co-optimization framework of these two models. At the start of the dynamic restoration stage ($t = t_3$), the RCD model is solved to dispatch repair crews to assigned faults. When a fault is cleared (considered as a repair event), a trigger signal is sent, indicating the availability of a repair crew. This triggers the next execution of the RCD model to dispatch the newly available repair crew. In this way, the RCD model is solved repeatedly in response to the clearance of a fault, by employing the MPC method. Simultaneously, the cleared fault allows the extension of the microgrids by energizing the branches and loads initially separated by the fault. Hence, the trigger signal also activates the initial execution of the SCLP model (indicated by the dashed arrow in green color), which selects cold loads that can be restored safely. Then the SCLP model runs dynamically to achieve sequential and secure load pickup. After each load pickup, the system condition is updated accordingly (indicated by the dashed arrow in blue color). The next execution of the SCLP model occurs when the system frequency returns to around the nominal value, indicating the completion of the frequency transient and the readiness of the ADN for the next step of cold load pickup.

The proposed co-optimization framework aims to provide seamless coordination between the RCD and SCLP models in low-inertia ADNs. To achieve this, new modeling techniques are adopted in this paper, including the event-driven formulation of the RCD model with MPC implementation, derivation of transient frequency constraints for the SCLP model, and co-optimization solution method. Mathematical formulations are detailed in the following sections.

III. Decision-Making of Event-Driven RCD

In order to address the novelty of the proposed RCD model compared to [3-15], the following assumptions are adopted:

1) All distribution lines (branches) and loads in the ADN are assumed to be equipped with a remote-controlled switch. The control time is negligible compared to the repair crew dispatch process that lasts for hours. This assumption is made for the purpose of focusing on the event-driven formulation and the incorporation of stochastic repair time in the proposed RCD model. Nevertheless, real-world scenarios are likely to be different. In cases where only a limited number of remote-controlled branch switches are installed, the proposed RCD model is still applicable by merging the uncontrollable branches and load nodes in an entire load zone, whose energization status is controlled by the adjacent remote-controlled switches [28].

On the other hand, when applying the proposed RCD model to a system with both manual and remote-controlled switches, the modeling techniques in [4] and [5] can be integrated without significant modification of the mathematical model. In such cases, the role of repair crews can be divided into two tasks: clearing faults and operating manual switches. The former task does not require any changes to the proposed model, while the latter can be addressed by incorporating a manual switch operation time into the energization process.

2) Only branch faults are considered, as faults at nodes (e.g., a fallen utility pole) can be formulated in the same way as branch faults, i.e., one can assign a "shared" fault to all branches adjacent to the faulted node. The branches are allowed to be energized only after the "shared" fault has been cleared.

Some explanations of the terms used in the RCD model are:

1) Recovery operation: An operation conducted by a repair crew to restore a faulted branch, indicated by $k \in \mathcal{K}$, comprises a transportation process and a fault clearance process.

2) Repair time (of a faulted branch): The duration required by a repair crew to fix the faulted branch, indicated by $t_{c,mn,k}$.

3) Restoration time (of a faulted branch): The time between 0 and the end of the restoration process T_{end}, when the faulted branch is back online, indicated by t_{mn}.

Based on the MPC, the RCD model is solved over a set of recovery operations $\mathcal{K} = \{1,2,\dots,|\mathcal{K}|\}$ ($|\mathcal{K}| \leq |\mathcal{E}_{\text{F}}|$), i.e., $|\mathcal{K}|$ future recovery operations are carried out in each MPC step.

A. Modeling of Repair Crew Dispatch

The dispatch of a repair crew to a faulted branch is formulated as $z_{c,mn,k}$, taking 1 if faulted branch (m,n) is fixed by repair crew c in the k^{th} recovery operation. The value of $z_{c,mn,k}$ is restricted by (1a) and (1b), imposing that only one faulted branch can be fixed in each recovery operation, and a faulted branch cannot be fixed more than once.

$$\sum_{(m,n)\in\mathcal{E}_{\text{F}}}\sum_{c\in\mathcal{C}} z_{c,nm,k} \leq 1, \quad \forall k \in \mathcal{K} \tag{1a}$$

$$\sum_{k\in\mathcal{K}}\sum_{c\in\mathcal{C}} z_{c,nm,k} \leq 1, \quad \forall (m,n) \in \mathcal{E}_{\text{F}} \tag{1b}$$

The binary variable $z_{c,mn,k}$ helps to sort the $|\mathcal{K}|$ recovery operations chronologically. The k^{th} recovery operation should be finished not earlier than the $(k-1)^{\text{th}}$ recovery operation, i.e.,

$$t^{\text{F}}_{k-1} \leq t^{\text{F}}_{k}, \quad \forall k \in \mathcal{K} \tag{1c}$$

$$t^{\text{F}}_{k} = \sum_{(m,n)\in\mathcal{E}_{\text{F}}}\sum_{c\in\mathcal{C}} z_{c,nm,k} t_{mn}, \quad \forall k \in \mathcal{K} \tag{1d}$$

where the finishing time of the k^{th} recovery operation t^{F}_{k} is the time instant when the specific faulted branch is restored in that recovery operation. In (1d), the value of t^{F}_{k} is obtained by the product of $z_{c,nm,k}$ and t_{mn}, as there is only one non-zero $z_{c,nm,k}$ throughout all faulted branches and repair crews in every recovery operation, as restricted by (1a).

B. Energized Network Identification

The system-level branch status after the k^{th} recovery operation, $y_{ij,k}$, is determined based on the following scenarios:

1) The consistently operating branches without faults, i.e.,

$$y_{ij,k} = 1, \quad \forall (i,j) \in \mathcal{E}_{\text{N}}, k \in \mathcal{K} \tag{2a}$$

2) The faulted branches, i.e.,

$$y_{ij,k} = \sum_{l=1}^{k}\sum_{c\in\mathcal{C}} z_{c,ij,l}, \quad \forall (i,j) \in \mathcal{E}_{\text{F}}, k \in \mathcal{K} \tag{2b}$$

The status of a faulted branch after the k^{th} recovery operation is set as 1, if a repair crew restores it in the k^{th} or previous recovery operations. Equation (2b) features system status when a recovery operation has finished. In this way, system changes are captured using a limited number of variables.

3) A de-energized branch without faults is allowed to be restored when there is at least one adjacent healthy branch, i.e.,

$$y_{ij,k} \leq \sum_{(a,b)\in\mathcal{E}_{ij}} y_{ab,k}, \quad \forall (i,j) \in \mathcal{E}_{\text{O}}, k \in \mathcal{K} \tag{2c}$$

Based on the above branch statuses, the restoration status of nodes after the k^{th} recovery operation is described as (2d), requiring the energization of the two end nodes ($x_{i,k} = x_{j,k} = 1$) of an energized branch ($y_{ij,k} = 1$).

$$\begin{cases} y_{ij,k} \leq x_{i,k} \\ y_{ij,k} \leq x_{j,k} \end{cases}, \quad \forall (i,j) \in \mathcal{E}, k \in \mathcal{K} \tag{2d}$$

C. Operating Constraints

For every recovery operation ($k \in \mathcal{K}$), the following constraints (3a)-(3f) are imposed for every possible change of the system state. Equations (3a) and (3b) are the power flow equations of the linearized DistFlow model [29], where the voltage magnitude and branch flow are calculated. The secure operating region, expressed by the upper and lower limits of the voltage magnitude and power flow, is described in (3c) and (3d).

$$\begin{cases} \sum\limits_{h:(h,i)\in\mathcal{E}} p_{hi,k} - \sum\limits_{j:(i,j)\in\mathcal{E}} p_{ij,k} = p^{\text{G}}_{i,k} - p^{\text{L}}_{i,k} \\ \sum\limits_{h:(h,i)\in\mathcal{E}} q_{hi,k} - \sum\limits_{j:(i,j)\in\mathcal{E}} q_{ij,k} = q^{\text{G}}_{i,k} - q^{\text{L}}_{i,k} \end{cases}, \quad \forall i \in \mathcal{N} \tag{3a}$$

$$\begin{cases} v_{i,k} - v_{j,k} \geq 2(R_{ij}p_{ij,k} + X_{ij}q_{ij,k}) - V^2_{\max}(1 - y_{ij,k}) \\ v_{i,k} - v_{j,k} \leq 2(R_{ij}p_{ij,k} + X_{ij}q_{ij,k}) + V^2_{\max}(1 - y_{ij,k}) \end{cases}, \quad \forall (i,j) \in \mathcal{E} \tag{3b}$$

$$V^2_{\min} x_{i,k} \leq v_{i,k} \leq V^2_{\max} x_{i,k}, \quad \forall i \in \mathcal{N} \tag{3c}$$

$$p^2_{ij,k} + q^2_{ij,k} \leq F^2_{ij,\max} y_{ij,k}, \quad \forall (i,j) \in \mathcal{E} \tag{3d}$$

Since the proposed RCD model focuses on assigning repair tasks to available crews, the DGs and loads are modeled simply as constant power injections. In (3e), the DGs' active and reactive power outputs are restricted within their operating limits. Electric loads are modeled in (3f) by their on/off switching state, and further requirements are imposed so that a load can be picked up only after energizing the node where it is connected, and a load should keep energized once it has been restored.

$$\begin{cases} P^{\text{G}}_{i,\min} x_{i,k} \leq p^{\text{G}}_{i,k} \leq P^{\text{G}}_{i,\max} x_{i,k} \\ (p^{\text{G}}_{i,k})^2 + (q^{\text{G}}_{i,k})^2 \leq (S^{\text{G}}_{i})^2 x_{i,k} \end{cases}, \quad \forall i \in \mathcal{N} \tag{3e}$$

$$\begin{cases} p^{\text{L}}_{i,k} = P^{\text{L}}_{i} x^{\text{L}}_{i,k}, \quad q^{\text{L}}_{i,k} = Q^{\text{L}}_{i} x^{\text{L}}_{i,k} \\ x^{\text{L}}_{i,k} \leq x_{i,k}, \qquad x^{\text{L}}_{i,k-1} \leq x^{\text{L}}_{i,k} \end{cases}, \quad \forall i \in \mathcal{N} \tag{3f}$$

D. Modeling of Stochastic Repair Time

Due to the inherent stochasticity of the fault clearance process, it is essential to account for the variable nature of repair time rather than treating it as a constant parameter. This paper proposes a dynamic evaluation of the stochastic repair time, utilizing two different approximations to capture the evolving availability of fault information to system operators.

After a major disruption occurs, the locations of faults can be determined shortly after the interruption, thanks to well-established fault diagnosis algorithms in ADNs. Additionally, transient voltage and current analysis enables an early classification of open-circuit and short-circuit faults. This valuable fault information is swiftly available and shared with the dispatch center following the emergency event. On this basis, a rough approximation can be developed to provide initial estimation of the stochastic repair time before dispatching repair crews.

Once the repair crews physically reach the fault area, they gain direct visibility of the ongoing failure and can assess the repair time more accurately based on the observed details, such as a broken conductor, fallen utility pole, or damaged insulator. In such case, the rough approximation is updated and replaced with a more accurate approximation. This refined estimation is carried out by the repair crews upon their arrival at the fault location, leveraging their expertise and the firsthand information gathered.

These two approximation techniques are detailed as:

1) Rough approximation: A statistics-based approach is employed to estimate the repair time required by repair crew c to clear the fault on faulted branch (m,n). Mathematically, the stochastic repair time is described by a mean $TR^{\text{avg}}_{c,mn}$ and a variance $TR^{\text{var}}_{c,mn}$. These values can be derived from historical performance data of the repair crews.

2) More accurate approximation: The truncated normal distribution [30] is utilized to describe the stochastic repair time in an informative manner. In addition to a mean $TA^{\text{avg}}_{c,mn}$ and a variance $TA^{\text{var}}_{c,mn}$, two estimations, one pessimistic and one optimistic, are integrated to describe the lower and upper bounds ($TA^{-}_{c,mn}$ and $TA^{+}_{c,mn}$) of the stochastic repair time.

On this basis, the stochastic repair time can be formulated as chance constraints with a desirable probability level ε, i.e.,

$$F(t_{c,mn,k}) \geq \varepsilon, \quad \forall c \in \mathcal{C}, (m,n) \in \mathcal{E}_{\text{F}}, k \in \mathcal{K} \tag{4a}$$

where $F(\bullet)$ is the *Cumulative Distribution Function* (CDF).

The repair time $t_{c,mn,k}$ is dynamically updated, according to the following procedure:

1) Before dispatching repair crews, the repair time $t_{c,mn,k}$ is determined by the rough approximation, i.e.,

$$t_{c,mn,k} \geq TR^{\text{avg}}_{c,mn} + \sqrt{\frac{\varepsilon}{1-\varepsilon}} TR^{\text{var}}_{c,mn} \tag{4b}$$

Equation (4b) is a deterministic surrogate of the chance constraint (4a), approximated by the Cantelli-Chebyshev inequality [31], which is guaranteed to hold for any distribution with the mean and variance provided as foreknowledge. The key advantage of surrogate (4b) is that it does not require a specific distribution, which is hard to obtain due to the long-tail feature of repair time [32].

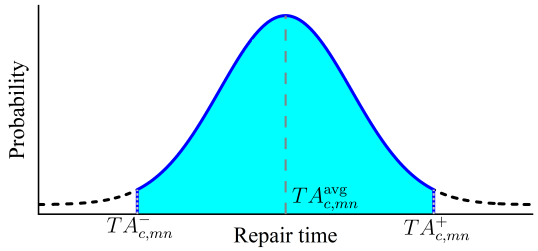

Fig. 3 The PDF of the stochastic repair time $t_{c,mn,k}$.

2) After a repair crew has arrived at the fault area and estimated the repair time, chance constraint (4a) can be convexified based on the more accurate approximation. Fig. 3 depicts the *Probability Density Function* (PDF) of the stochastic repair time $t_{c,mn,k}$, which follows a truncated normal distribution within the interval $[TA^{-}_{c,mn}, TA^{+}_{c,mn}]$. According to [30], the inverse CDF of $t_{c,mn,k}$ can be expressed as

$$F^{-1}_{c,mn}(\varepsilon) = TA^{\text{avg}}_{c,mn} + \Phi^{-1}(\kappa\varepsilon + \Phi(\alpha_1))\sqrt{TA^{\text{var}}_{c,mn}} \tag{4c}$$

where $\Phi(\bullet)$ and $\Phi^{-1}(\bullet)$ are the CDF and inverse CDF of the standard normal distribution, respectively; κ, α_1, and α_2 are introduced parameters with the following expressions.

$$\begin{cases} \kappa = \Phi(\alpha_2) - \Phi(\alpha_1) \\ \alpha_1 = (TA^{-}_{c,mn} - TA^{\text{avg}}_{c,mn}) \big/ \sqrt{TA^{\text{var}}_{c,mn}} \\ \alpha_2 = (TA^{+}_{c,mn} - TA^{\text{avg}}_{c,mn}) \big/ \sqrt{TA^{\text{var}}_{c,mn}} \end{cases} \tag{4d}$$

Therefore, the following linear constraint on the stochastic repair time $t_{c,mn,k}$ can be derived by inverting both sides of (4a).

$$\begin{aligned} t_{c,mn,k} &\geq F^{-1}_{c,mn}(\varepsilon) \\ &= TA^{\text{avg}}_{c,mn} + \Phi^{-1}(\kappa\varepsilon + \Phi(\alpha_1))\sqrt{TA^{\text{var}}_{c,mn}} \end{aligned} \tag{4e}$$

E. Modeling of Restoration Time

Given the repair time $t_{c,mn,k}$ above, the restoration time of faulted branch (m,n) can be obtained by the three terms in (5a): 1) the repair time required to fix branch (m,n); 2) the past time before repairing branch (m,n), including the restoration time of the previously restored branch and the transportation time, if branch (m,n) is not first restored; 3) the transportation time from the repair station/depot, if branch (m,n) is restored first.

$$t_{mn} \geq t^{\text{re}}_{mn} + t^{\text{pr}}_{mn} + t^{\text{tr}}_{mn}, \quad \forall (m,n) \in \mathcal{E} \tag{5a}$$

$$\begin{cases} t^{\text{re}}_{mn} = \sum\limits_{k\in\mathcal{K}} \sum\limits_{c\in\mathcal{C}} z_{c,mn,k} t_{c,mn,k} \\ t^{\text{pr}}_{mn} = \sum\limits_{(i,j)\in\mathcal{E}_{\text{F}}} w_{ij,mn}(t_{ij} + T^{\text{tr}}_{ij,mn}), \quad \forall (m,n) \in \mathcal{E} \\ t^{\text{tr}}_{mn} = w_{0,mn} T^{\text{tr}}_{0,mn} \end{cases} \tag{5b}$$

Similar to (1d), the repair time t^{re}_{mn} is obtained by summing the products of $z_{c,mn,k}$ and $t_{c,mn,k}$, shown as the first equation of (5b). In the second equation, $w_{ij,mn}$ takes 1 only if the restoration of branch (m,n) follows branch (i,j) by the same repair crew, and the previous past time t^{pr}_{mn} is expressed as the sum of the restoration time of the preciously restored branch

(i,j) and the transportation time from branch (i,j) to branch (m,n). Lastly, whether branch (m,n) is first restored is indicated by the value of $w_{0,mn}$. The following constraints are imposed on $w_{ij,mn}$ and $w_{0,mn}$.

$$\begin{cases} \sum\limits_{(i,j)\in\mathcal{E}_\mathrm{F}} w_{ij,mn} = \sum\limits_{k\in\mathcal{K}}\sum\limits_{c\in\mathcal{C}} z_{c,mn,k} - w_{0,mn} \\ \sum\limits_{(i,j)\in\mathcal{E}_\mathrm{F}} w_{mn,ij} \le \sum\limits_{k\in\mathcal{K}}\sum\limits_{c\in\mathcal{C}} z_{c,mn,k} \\ w_{mn,mn} = 0 \end{cases}, \forall (m,n)\in\mathcal{E}_\mathrm{F} \tag{5c}$$

$$w_{ij,mn} \le \sum_{k\in\mathcal{K}}\sum_{c\in\mathcal{C}} \left(z_{c,mn,k} \sum_{l=1}^{k-1} z_{c,ij,l} \right), \forall (i,j),(m,n)\in\mathcal{E}_\mathrm{F} \tag{5d}$$

$$\sum_{(m,n)\in\mathcal{E}_\mathrm{F}} w_{0,mn} \le |\mathcal{C}| \tag{5e}$$

Equation (5c) requires that every faulted branch has one predecessor and one successor in the restoration sequence, except the first and last one to be restored. The value of $w_{ij,mn}$ is next restricted by (5d), where it takes 1 only if the restoration of branch (m,n) follows branch (i,j) by the same repair crew. Lastly, the number of first restored branches should be less than that of repair crews, shown as (5e).

It is worth noting that the product of a binary variable and an arbitrary variable can be linearized using the big-M method [33]. Hence, equations (1d), (5b), and (5d) are intrinsically linear. The linearization process is detailed as follows.

For (1d), an auxiliary variable $a^1_{c,mn,k} = z_{c,mn,k} t_{mn}$ is introduced. Then $a^1_{c,mn,k}$ is restricted by (6a), where the first and second constraints require $a^1_{c,mn,k} = t_{mn}$ when $z_{c,mn,k} = 1$, and the third enforces $a^1_{c,mn,k} = 0$ when $z_{c,mn,k} = 0$.

$$\begin{cases} a^1_{c,mn,k} \ge t_{mn} - T_\mathrm{end}(1 - z_{c,mn,k}) \\ a^1_{c,mn,k} \le t_{mn} + T_\mathrm{end}(1 - z_{c,mn,k}) \\ -T_\mathrm{end} z_{c,mn,k} \le a^1_{c,mn,k} \le T_\mathrm{end} z_{c,mn,k} \end{cases} \tag{6a}$$

Hence, equation (1d) is linearized as

$$t^\mathrm{F}_k = \sum_{(m,n)\in\mathcal{E}_\mathrm{F}} \sum_{c\in\mathcal{C}} a^1_{c,mn,k}, \quad \forall k\in\mathcal{K} \tag{6b}$$

Similarly, equation (5b) is replaced by (7a)-(7c), using variables $a^2_{c,mn,k} = z_{c,mn,k} t_{c,mn,k}$ and $a^3_{ij,mn} = w_{ij,mn} t_{ij}$.

$$\begin{cases} t^\mathrm{re}_{mn} = \sum\limits_{k\in\mathcal{K}}\sum\limits_{c\in\mathcal{C}} a^2_{c,mn,k} \\ t^\mathrm{pr}_{mn} = \sum\limits_{(i,j)\in\mathcal{E}_\mathrm{F}} \left(a^3_{ij,mn} + w_{ij,mn} T^\mathrm{tr}_{ij,mn} \right), \\ t^\mathrm{tr}_{mn} = w_{0,mn} T^\mathrm{tr}_{0,mn} \end{cases} \forall (m,n)\in\mathcal{E} \tag{7a}$$

$$\begin{cases} a^2_{c,mn,k} \ge t_{c,mn,k} - T_\mathrm{end}(1 - z_{c,mn,k}) \\ a^2_{c,mn,k} \le t_{c,mn,k} + T_\mathrm{end}(1 - z_{c,mn,k}) \\ -T_\mathrm{end} z_{c,mn,k} \le a^2_{c,mn,k} \le T_\mathrm{end} z_{c,mn,k} \end{cases} \tag{7b}$$

$$\begin{cases} a^3_{ij,mn} \ge t_{ij} - T_\mathrm{end}(1 - w_{ij,mn}) \\ a^3_{ij,mn} \le t_{ij} + T_\mathrm{end}(1 - w_{ij,mn}) \\ -T_\mathrm{end} w_{ij,mn} \le a^3_{ij,mn} \le T_\mathrm{end} w_{ij,mn} \end{cases} \tag{7c}$$

Lastly, equation (5d) is linearized as (8a) and (8b), where the "big M" is set as 1, also the upper bound of the introduced variable $a^4_{c,ij,mn,k} = z_{c,mn,k} \sum_{l=1}^{k-1} z_{c,ij,l}$.

$$w_{ij,mn} \le \sum_{k\in\mathcal{K}}\sum_{c\in\mathcal{C}} a^4_{c,ij,mn,k}, \quad \forall (i,j),(m,n)\in\mathcal{E}_\mathrm{F} \tag{8a}$$

$$\begin{cases} a^4_{c,ij,mn,k} \ge \sum\limits_{l=1}^{k-1} z_{c,ij,l} - (1 - z_{c,mn,k}) \\ a^4_{c,ij,mn,k} \le \sum\limits_{l=1}^{k-1} z_{c,ij,l} + (1 - z_{c,mn,k}) \\ -z_{c,mn,k} \le a^4_{c,ij,mn,k} \le z_{c,mn,k} \end{cases} \tag{8b}$$

F. Objective Function

The proposed RCD model aims to maximize the capacity of energized loads by the optimal repair crew dispatch, i.e.,

$$\max \sum_{k\in\mathcal{K}}\sum_{i\in\mathcal{N}} \lambda_i (p^\mathrm{L}_{i,k} - p^\mathrm{L}_{i,k-1})(T_\mathrm{end} - t^\mathrm{F}_k) \tag{9}$$

In (9), $(p^\mathrm{L}_{i,k} - p^\mathrm{L}_{i,k-1})$ and $(T_\mathrm{end} - t^\mathrm{F}_k)$ are the restored load power in the k^th recovery operation and its duration.

IV. Decision-Making of Sequential Cold Load Pickup

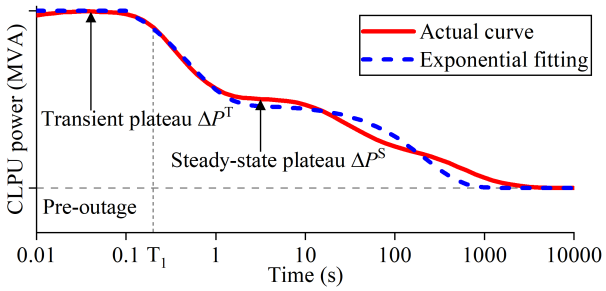

Fig. 4 A real-world cold load pickup example in [16] and its exponential fitting.

The proposed SCLP model aims to demonstrate whether a cold load pickup operation complies with the security constraints for frequency dynamics and steady-state operations (power flow-based security). These constraints are coordinated by considering the transition of cold load pickup demands between the transient and steady-state plateaus, as illustrated in Fig. 4. It should be noted that the proposed SCLP model focuses on determining a secure cold load pickup sequence, while power management schemes such as economic operating and scheduling can be further considered in subsequent steps [34].

Required variables in the SCLP model involve switching operations (x_i, y_{ij}, x^L_i) and the steady-state power flow (p_{ij}, q_{ij}, p^G_i, q^G_i, p^L_i, q^L_i, v_i), which have the same meaning as those in the RCD model with the subscript k discarded. System frequency dynamics can be derived based on these variables.

A. Modeling of Cold Load Pickup

As shown in the CLPU report [16], the CLPU demand obtained by realistic tests can be generally described by Fig. 4. As shown, the CLPU demand reaches the peak value quickly after energization, due to transient inrush current. The typical duration of the peak transient plateau is 0.2-0.4 s [16]. Shortly after

this, the CLPU demand approaches the steady state and decreases gradually afterward. During the steady state, the loss of load diversity mainly causes the higher-than-normal load demand. The power of the steady-state plateau is typically 40% to 60% of the transient plateau, depending on load types, weather conditions, and outage duration. The CLPU effect vanishes as the demand reaches the pre-outage value.

The dashed line in blue color in Fig. 4 provides an exponential fitting of the actual curve, which is adequately accurate for modeling the CLPU power. However, the accuracy is based on fitting the curve after actual measurement data is already available [19]. This data highly depends on the specific condition before CLPU, and the fitted curve based on historical data might lead to inaccuracy [19]. Nevertheless, evaluating the magnitude of the peak demand (transient plateau) is generally considered accurate, as indicated by a realistic prediction example in [16] and the quantitative analysis in [19].

This paper proposes a novel CLPU model based on the transition between the transient and steady-state plateaus. The ratio of the two plateaus is denoted as ρ. The CLPU model proposed in (10a) uses the peak demand in the transient stage ($t < T_1$) and the steady-state demand of the second plateau ($t \geq T_1$). The two demands are necessary to formulate the transient performance (frequency dynamics) and steady-state security (power flow).

$$p_i^{\mathrm{L}} = \big(u(t) - u(t-T_1)\big)P_i^{\mathrm{T}} + u(t-T_1)P_i^{\mathrm{S}} = p_i^{\mathrm{T}} + p_i^{\mathrm{S}} \quad (10a)$$

where p_i^{L} is the CLPU demand at node i, comprising a transient power p_i^{T} and a steady-state power p_i^{S}; $u(t)$ is the step function.

The CLPU demand at the system level is then formulated as

$$\begin{aligned}\Delta P^{\mathrm{L}} &= \sum_{i\in\mathcal{N}}(x_i^{\mathrm{L}} - x_{i,0}^{\mathrm{L}})p_i^{\mathrm{L}} \\ &= \sum_{i\in\mathcal{N}}(x_i^{\mathrm{L}} - x_{i,0}^{\mathrm{L}})\left(u(t)P_i^{\mathrm{T}} + u(t-T_1)(P_i^{\mathrm{S}} - P_i^{\mathrm{T}})\right) \quad (10b) \\ &= u(t)\Delta P^{\mathrm{T}} + u(t-T_1)(\Delta P^{\mathrm{S}} - \Delta P^{\mathrm{T}})\end{aligned}$$

where ΔP^{T} and ΔP^{S} are the transient and steady-state CLPU demand at the system level, respectively.

B. Frequency-Constrained Cold Load Pickup

The high penetration of inverter-interfaced DGs results in low-inertia ADNs, as the fast-acting power inverters electrically decouple the rotational kinetic energy stored in the rotor of turbine-interfaced generators from the system, if any. Maintaining frequency stability is crucial in low-inertia systems, as the fast-changing frequency dynamics may undesirably trigger protection to shed loads and generators.

The SCLP model focuses on system-level security, so the swing equation of *Center-of-Inertia* (CoI) [35] is used to model the frequency dynamics, as shown in (11). It should be noted that the inertia constant M and damping constant D in (11) should be obtained considering the energized part of the ADN.

$$M\frac{d\Delta f}{dt} + D\Delta f = \Delta P^{\mathrm{G}} - \Delta P^{\mathrm{L}} \quad (11)$$

ΔP^{G} and ΔP^{L} are the generation power increase and restored load power, respectively.

1) Rate of Change of Frequency

The RoCoF is derived by solving (11) at the very instant of load pickup, when the frequency deviation Δf and generation power increase ΔP^{G} are considered as 0. Considering the CLPU feature, the RoCoF is constrained by the transient plateau in Fig. 4, i.e.,

$$|\mathrm{RoCoF}| = \left|\frac{-\Delta P^{\mathrm{L}}}{M}\right| = \frac{\Delta P^{\mathrm{T}}}{M} \leq \mathrm{RoCoF}_{\max} \quad (12)$$

2) Transient Frequency Nadir

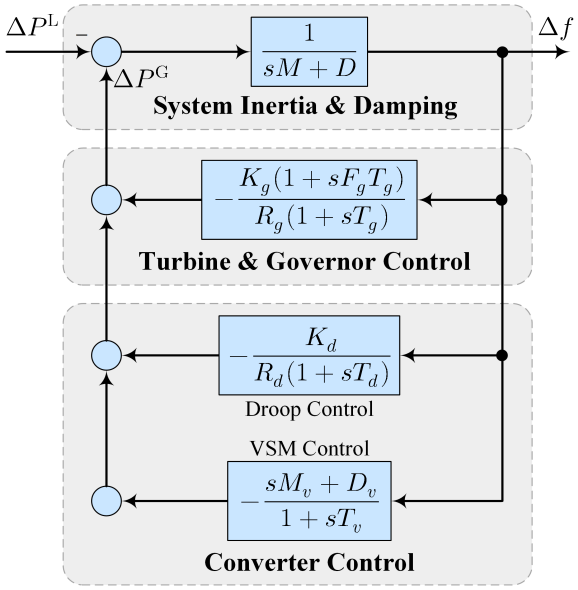

Fig. 5 Uniform frequency response model for low-inertia systems [21].

In the context of ADNs, the active power increase ΔP^{G} is a result of the governor control of synchronous generators and frequency control of inverter-interfaced DGs. The droop and *Virtual Synchronous Machine* (VSM) control schemes are considered in this paper to formulate ΔP^{G} in a general manner. The simplified, but sufficiently accurate, uniform frequency response model for low-inertia systems [21] is adopted, as shown in Fig. 5. For a synchronous generator $g \in \mathcal{G}$, R_g and K_g are the respective droop and mechanical power gain factor, while T_g and F_g denote the turbine time constant and the fraction of total power generated by the turbine, respectively. Inverter-interfaced DGs do not have a complicated gas or water turbine, and their power adjustment relies mainly on the responsive droop control. For instance, the frequency response of a droop-controlled DG $d \in \mathcal{D}$ can be expressed by the gain K_d, the slope R_d, and the time constant T_d of the droop. Furthermore, the synthetic inertia M_v and damping D_v of a VSM-based DG $v \in \mathcal{V}$ are introduced with the time constant T_v .

By assuming equal time constants for all synchronous machines ($T_g = T, \forall g \in \mathcal{G}$) and neglecting the much smaller inverter time constants ($T \gg T_d \approx T_v \approx 0, \forall d \in \mathcal{D}, v \in \mathcal{V}$), the frequency deviation can be expressed as in (13a), using the auxiliary parameters shown in (13b).

$$\Delta f = -\frac{\Delta P^{L}}{M_s T}\frac{1+sT}{s^2 + 2\zeta\omega_n s + \omega_n^2} \quad (13a)$$

$$\begin{cases} M_s = M + \sum_{v\in\mathcal{V}} M_v \,, D_s = D + \sum_{v\in\mathcal{V}} D_v \\ \omega_n = \sqrt{\dfrac{1}{M_s T}\left(D_s + \sum_{g\in\mathcal{G}} \dfrac{K_g}{R_g} + \sum_{d\in\mathcal{D}} \dfrac{K_d}{R_d}\right)} \\ \zeta = \dfrac{M_s + T\left(D_s + \sum_{g\in\mathcal{G}} \dfrac{K_g F_g}{R_g} + \sum_{d\in\mathcal{D}} \dfrac{K_d}{R_d}\right)}{2\sqrt{M_s T\left(D_s + \sum_{g\in\mathcal{G}} \dfrac{K_g}{R_g} + \sum_{d\in\mathcal{D}} \dfrac{K_d}{R_d}\right)}} \end{cases} \tag{13b}$$

By inserting (10b) into (13a), the frequency nadir Δf^{ndr} is

$$\Delta f^{\mathrm{ndr}} = -\frac{1}{M_s T \omega_n^2}\Delta P^{\mathrm{S}} + \frac{h(t_n)}{M_s T \omega_n \omega_b}\Delta P^{\mathrm{T}} + \frac{h(t_n - T_1)}{M_s T \omega_n \omega_b}(\Delta P^{\mathrm{S}} - \Delta P^{\mathrm{T}}) \tag{13c}$$

, where

$$\begin{cases} h(t) = u(t) e^{-\zeta\omega_n t}(\sin(\omega_b t + \phi) - \omega_n T \sin(\omega_b t)) \\ \omega_b = \omega_n\sqrt{1-\zeta^2}, \phi = \arctan\left(\sqrt{(1-\zeta^2)}/\zeta\right) \\ \varphi = \dfrac{\omega_b + \chi\left((\zeta\omega_n - T^{-1})\beta_1 + \omega_b\beta_2\right)}{(\zeta\omega_n - T^{-1}) + \chi\left((\zeta\omega_n - T^{-1})\beta_2 - \omega_b\beta_1\right)} \\ t_n = \dfrac{1}{\omega_b}\arctan(\varphi)\,, \chi = (\rho-1)e^{\zeta\omega_n T_1} \\ \beta_1 = \sin(\omega_b T_1)\,, \beta_2 = \cos(\omega_b T_1) \end{cases} \tag{13d}$$

It is worth noting that Δf^{ndr} in (13c) is a linear expression of ΔP^{T} and ΔP^{S}, which are also linear expressions of the load energization variables x_i^{L}. Thus, the following frequency nadir constraint is linear.

$$|\Delta f^{\mathrm{ndr}}| \le \Delta f_{\max}^{\mathrm{ndr}} \tag{13e}$$

3) Quasi-Steady-State Frequency

The constraint for assuring the steady-state frequency security can be obtained from (11) by assuming that $d\Delta f/dt$ is 0 after the transient state is over. In this stage, only the steady-state CLPU demand ΔP^{S} is considered, and the steady-state generation power increase ΔP^{G} is determined based on the *Final Value Theorem* (FVM), detailed as

$$\Delta P^{\mathrm{G}} = \left(-\sum_{g\in\mathcal{G}}\frac{R_g}{K_g} - \sum_{d\in\mathcal{D}}\frac{R_d}{K_d} - \sum_{v\in\mathcal{V}} D_v\right)\Delta f^{\mathrm{ss}} \tag{14a}$$

By combining (14a) and (11), the steady-state frequency deviation Δf^{ss} can be expressed as

$$|\Delta f^{\mathrm{ss}}| = \frac{\Delta P^{\mathrm{S}}}{D_s + \sum_{g\in\mathcal{G}}\dfrac{R_g}{K_g} + \sum_{d\in\mathcal{D}}\dfrac{R_d}{K_d}} \le \Delta f_{\max}^{\mathrm{ss}} \tag{14b}$$

C. Steady-State Power Flow

The operating constraints (3a)-(3e) are again used to formulate steady-state security. The only difference is that the subscript k is discarded, and load demand p_i^{L} is expressed as steady-state CLPU demand $p_i^{\mathrm{S}} x_i^{\mathrm{L}}$. For simplicity, these constraints are not duplicated here.

D. Switching Operations

The SCLP model determines the switching operations for the outage nodes, branches, and loads. Similar to (2a)-(2d), the following constraints are developed:

$$\begin{cases} y_{ij} = 1, & \forall (i,j) \in \mathcal{E}_{\mathrm{N}} \\ y_{ij} = 0, & \forall (i,j) \in \mathcal{E}_{\mathrm{F}} \\ y_{ij} \le \sum_{(a,b)\in E_{ij}} y_{ab}\,, & \forall (i,j) \in \mathcal{E}_{\mathrm{O}} \\ y_{ij} \le x_i, y_{ij} \le x_j, & \forall (i,j) \in \mathcal{E} \\ x_i^{\mathrm{L}} \le x_i, & \forall i \in \mathcal{N} \end{cases} \tag{15a}$$

It should be noted that the set $\mathcal{E}_{\mathrm{N}}$, $\mathcal{E}_{\mathrm{F}}$, and $\mathcal{E}_{\mathrm{O}}$ are updated dynamically with the implementation of the RCD model.

Based on different outage conditions, a final topology ($x_{i,\infty}$, $y_{ij,\infty}$, and $x_{i,\infty}^{\mathrm{L}}$) of the restored ADN should be provided prior to executing the restoration plan. Specifically, $x_{i,\infty}$, $y_{ij,\infty}$, and $x_{i,\infty}^{\mathrm{L}}$ are all considered as 1, if the primary transformer functions normally, despite faults happening within the ADN. Otherwise, the ADN can form *Microgrids* (MG) [36] and the values of $x_{i,\infty}$, $y_{ij,\infty}$, and $x_{i,\infty}^{\mathrm{L}}$ need to be set accordingly. On this basis, the energization statuses are further constrained by:

$$\begin{cases} y_{ij} \le y_{ij,\infty}, & \forall (i,j) \in \mathcal{E} \\ x_i \le x_{i,\infty}, & \forall i \in \mathcal{N} \\ x_i^{\mathrm{L}} \le x_{i,\infty}^{\mathrm{L}}, & \forall i \in \mathcal{N} \end{cases} \tag{15b}$$

E. Objective Function

The SCLP model aims to restore the most loads per step, i.e.,

$$\max \sum_{i\in\mathcal{N}} P_i^{\mathrm{L}}(x_i^{\mathrm{L}} - x_{i,0}^{\mathrm{L}}) \tag{16}$$

Mathematically, the proposed RCD and SCLP models are formulated as a *Second-Order Cone Program* (SOCP) that can be solved efficiently by off-the-shelf commercial solvers.

The proposed dynamic ADN restoration strategy is applicable regardless of whether the primary transformer is disconnected or remains connected. When the primary transformer is in operation, it can be considered as a synchronous machine with high inertia and bulk capacity, thus dominating the frequency response. In this case, the frequency response model of the primary transformer is included as the dominant part of the "Turbine & Governor Control" in Fig. 5, and the mathematical formulation of frequency dynamics (12)-(14b) is updated accordingly to reflect this configuration.

However, it is important to note that the focus of this paper is primarily on the scenario where the primary transformer is disconnected. In this case, the ADN relies on the available DGs for frequency regulation. The proposed restoration strategy specifically addresses the challenges related to picking up cold loads in low-inertia ADNs where the primary transformer is lost. Thus, the proposed strategy contributes mainly to sequential restoration of cold loads in low-inertia ADNs.

V. Solution Methodology

The proposed dynamic ADN restoration strategy is detailed in Fig. 6 with the following steps:

[**s1**] Acquire initial conditions of the ADN, including network parameters, fault locations, and frequency control parameters.

[**s2**] Set the current step for repair crew dispatch $s_{\mathrm{rcd}} = 0$.

[**s3**] Before sending out repair crews, obtain the rough approximation of each faulted branch's repair time required by every repair crew ($TR^{\mathrm{avg}}_{c,mn}$ and $TR^{\mathrm{var}}_{c,mn}$).

[**s4**] Obtain the real-time transportation information ($T^{\mathrm{tr}}_{ij,mn}$ and $T^{\mathrm{tr}}_{0,mn}$) for the current crew dispatch step s_{rcd}.

[**s5**] For the initial step $s_{\mathrm{rcd}} = 0$, solve the RCD model with the rough approximation of repair time, then go to [**s8**]; for the following steps $s_{\mathrm{rcd}} \geq 1$, go to [**s6**].

[**s6**] Check if any repair crews arrived at the fault area; if yes, obtain the more accurate approximation of repair time for those repair crews ($TA^{\mathrm{avg}}_{c,mn}$, $TA^{\mathrm{var}}_{c,mn}$, $TA^{-}_{c,mn}$ and $TA^{+}_{c,mn}$).

[**s7**] Solve the RCD model with the updated and more accurate approximation of repair time.

[**s8**] Send out the available repair crews to their designated faulted areas based on the solution result.

[**s9**] Check if a faulted branch has been restored; if yes, update the fault branch set $\mathcal{E}_{\mathrm{F}}$ and send out the trigger signal, then set $s_{\mathrm{rcd}} = s_{\mathrm{rcd}} + 1$ and go back to [**s4**] when there are still faults ($|\mathcal{E}_{\mathrm{F}}| \geq 1$); otherwise, wait for a while and repeat [**s9**].

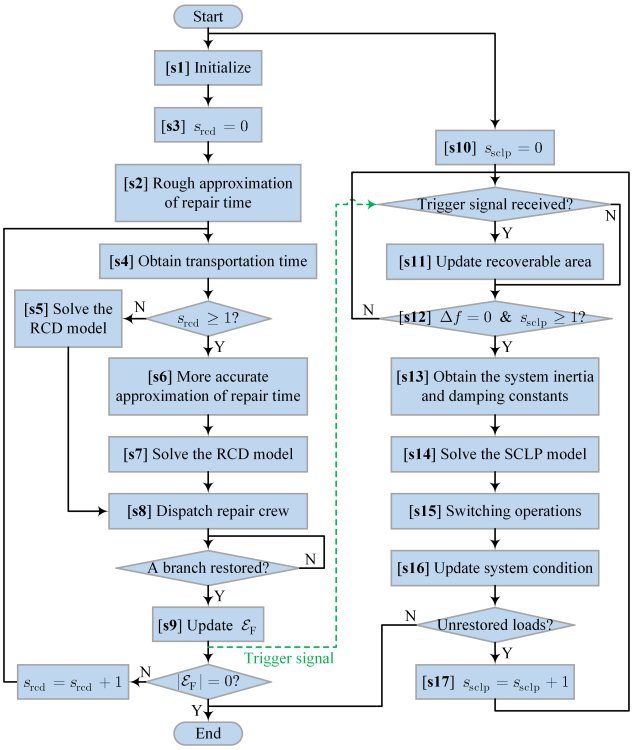

Fig. 6 Solution flowchart of the proposed dynamic ADN restoration strategy.

The following steps will be executed after the SCLP model receives the trigger signal for the first time:

[**s10**] Set the current step for load pickup $s_{\mathrm{sclp}} = 0$.

[**s11**] Check if the trigger signal is received; if yes, update the recoverable area of the ADN ($\mathcal{E}_{\mathrm{F}}$ and $\mathcal{E}_{\mathrm{O}}$).

[**s12**] Check if the system frequency is in steady state within limits; if not, wait for a while and go back to [**s11**].

[**s13**] Update the system inertia and damping constants M and D based on the energized area of the ADN.

[**s14**] Solve the SCLP model based on the updated sets and parameters in [**s11**] and [**s13**].

[**s15**] Switch on the designated nodes, branches, and loads based on the solution result.

[**s16**] Update system conditions ($\mathcal{E}_{\mathrm{O}}$ and $\mathcal{E}_{\mathrm{N}}$) after executing the load pickup in [**s15**].

[**s17**] If there are remaining loads to be picked up, set $s_{\mathrm{sclp}} = s_{\mathrm{sclp}} + 1$ and go back to [**s11**].

VI. Numerical Results

The effectiveness of the proposed dynamic ADN restoration strategy is verified in two study cases with different outage conditions:

A) A modified IEEE 33-node test feeder [37] with the primary transformer in service.

B) A modified real-world 136-node test feeder [38] with the primary transformer out of service.

Parameters applied in both cases are specified as follows. The minimum and maximum voltage magnitudes are set as 0.9 and 1.1 p.u., respectively. The weight coefficients of CLs and normal loads are set as 1 and 0.1, respectively. The magnitude of the transient and steady-state CLPU plateaus is set as 5 and 2.5 times higher than the pre-outage demand, respectively. The duration of the transient plateau is set as 0.3 s. The maximum RoCoF, allowed frequency nadir, and maximum steady-state frequency deviation are set as 1 Hz/s, 0.7 Hz, and 0.5 Hz, respectively. It is assumed that the system frequency will return to the normal state 10 min after each load pickup, which is typical for the secondary frequency control. While in the actual implementation of the proposed model, this time is the instant when the system frequency is restored. The optimization problems are solved by commercial solver Gurobi on a PC with an Intel Core i9-12900K processor and 64 GB RAM.

A. IEEE 33-Node Test Feeder

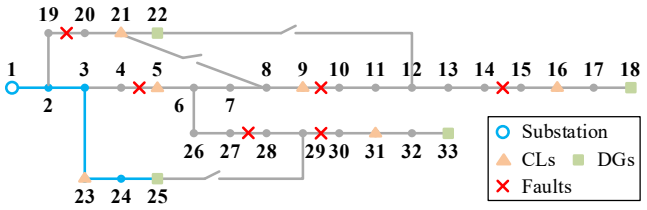

Fig. 7 The initial condition of the faulted IEEE 33-node test feeder.

The faulted condition of the IEEE 33-node system is shown in Fig. 7. There are 6 permanent branch faults, resulting in a small area (depicted in blue color) to be supplied by the substation. The outage area is shown in grey color. The number of repair crews is 2, both of which are initially located at one repair station. The transportation time between the repair station and the faulted branches is listed in TABLE II. The rough and more accurate approximation of the stochastic repair time is indicated in TABLE III. It is assumed that the rough and more accurate approximations share the same mean and variance.

This case focuses on the collaboration of the RCD and SCLP models, so it is assumed that all the DGs operate in the grid-following mode and do not respond to frequency changes, i.e.,

$\mathcal{D}=\mathcal{V}=\emptyset$. The system inertia and frequency response are provided only by the rotating generator at the substation at node 1. The system inertia $M = 10$ s at a 10 MW base, and the system damping $D = 1$. The governor and turbine control parameters are specified at the same 10 MW base: $K_g = 1$, $R_g = 0.05$, $F_g = 0.3$, and $T_g = 7$ s.

TABLE II Transportation time between the repair station and faulted branches

From / To	Repair station	(4, 5)	(9, 10)	(14, 15)	(19, 20)	(26, 27)	(29, 30)
Repair station	\	13	12	25	20	8	22
(4, 5)	13	\	18	15	22	19	16
(9, 10)	12	18	\	23	21	15	24
(14, 15)	25	15	23	\	11	9	19
(19, 20)	20	22	21	11	\	15	17
(26, 27)	8	19	15	9	15	\	21
(29, 30)	22	16	24	19	17	21	\

* All numbers are in min

TABLE III The rough and more accurate approximation of repair time

Faulted branches			(4, 5)	(9, 10)	(14, 15)	(19, 20)	(26, 27)	(29, 30)
Rough approximation	Mean	Crew 1	21	20	24	18	11	29
		Crew 2	15	23	18	30	28	26
	Var.[1]	Crew 1	17.64	16.00	23.04	12.96	4.84	33.64
		Crew 2	9.00	21.16	12.96	36.00	31.36	27.04
More accurate approximation	Opt.[2]	Crew 1	17	16	19	14	9	23
		Crew 2	12	18	14	24	22	21
	Pes.[2]	Crew 1	25	24	29	22	13	35
		Crew 2	18	28	22	36	34	31

[1] All numbers are in min except the variance (Var.) which is in min^2
[2] Opt. and Pes. indicate the optimistic and pessimistic estimation

Fig. 8 compares the restoration decisions determined by the proposed RCD model and a traditional multi-time-step model [18] that assumes a fixed interval of 20 min for ease of comparison. Model [18] provides a fault-clearing sequence without considering the transportation issue and varying difficulty levels of the fault-clearing process. In practice, strict compliance with this sequence may lead to suboptimality, due to the assumption that all faulted branches can be restored in a fixed interval. Specifically, model [18] suggests to restore branches (4, 5), (29, 30), (9, 10), (14, 15), (19, 20), and (27, 28) in order, while considering transportation and repair crews' ability, the optimal restoration sequence provided is (4, 5), (29, 30), (14, 15), (9, 10), (27, 28), and (19, 20), as proposed by the RCD model.

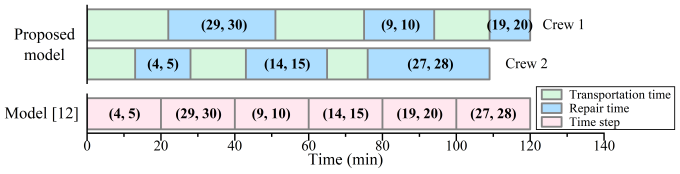

Fig. 8 Restoration sequence determined by the proposed RCD model and the multi-time-step model [18].

The full execution of the RCD and SCLP models is detailed in TABLE IV. As shown, branch (4, 5) is first restored at the 28th min, sending simultaneously the trigger signal. Subsequentially, the SCLP model is executed repeatedly to pick up loads. The cold load pickups during 28-48 min are depicted in Fig. 9. Initially, the loads at nodes 1-3 and 23-25 are energized by the substation. After faulted branch (4, 5) is restored, there are loads at nodes 4-13, 21, 22, and 26 to be picked up. The proposed SCLP model determines optimally that the loads at nodes 5, 7, 11, and 21 are restored first at the 28$^{\text{th}}$ min. After the system frequency returns to normal state 10 min later, the loads at nodes 4, 6, 12, 22, and 26 are restored at the 38$^{\text{th}}$ min. When the frequency is normal again (the 48$^{\text{th}}$ min), the loads at nodes 8 and 13 are restored. Note that another trigger signal is sent out at the 51$^{\text{st}}$ min when branch (29, 30) is restored, the SCLP model is solved with updated conditions that the loads at nodes 30-33 are ready to be energized. The subsequent clod load pickups are shown in TABLE IV.

TABLE IV Sequential cold load pickups in the IEEE 33-node test feeder

Time instant	Load pickup	Pre-outage demand (MW)	Cold load demands (MW)	Frequency dynamics
Branch (4, 5) is restored at the 28$^{\text{th}}$ min				
28 min	5, 7, 11, 21	0.40	$\Delta P^{\text{T}} = 1.98$ $\Delta P^{\text{S}} = 0.99$	RoCoF $= -0.99$ Hz/s $\Delta f^{\text{ndr}} = -0.53$ Hz $\Delta f^{\text{ss}} = -0.25$ Hz
Branch (29, 30) is restored at the 51$^{\text{st}}$ min				
38 min	4, 6, 12, 22, 26	0.39	$\Delta P^{\text{T}} = 1.95$ $\Delta P^{\text{S}} = 0.98$	RoCoF $= -0.98$ Hz/s $\Delta f^{\text{ndr}} = -0.53$ Hz $\Delta f^{\text{ss}} = -0.24$ Hz
48 min	8, 13	0.26	$\Delta P^{\text{T}} = 1.30$ $\Delta P^{\text{S}} = 0.65$	RoCoF $= -0.65$ Hz/s $\Delta f^{\text{ndr}} = -0.35$ Hz $\Delta f^{\text{ss}} = -0.16$ Hz
Branch (14, 15) is restored at the 65$^{\text{th}}$ min				
58 min	31, 32	0.36	$\Delta P^{\text{T}} = 1.80$ $\Delta P^{\text{S}} = 0.90$	RoCoF $= -0.90$ Hz/s $\Delta f^{\text{ndr}} = -0.48$ Hz $\Delta f^{\text{ss}} = -0.22$ Hz
Branch (9, 10) is restored at the 94$^{\text{th}}$ min				
68 min	14, 16, 18, 29	0.39	$\Delta P^{\text{T}} = 1.95$ $\Delta P^{\text{S}} = 0.98$	RoCoF $= -0.98$ Hz/s $\Delta f^{\text{ndr}} = -0.52$ Hz $\Delta f^{\text{ss}} = -0.24$ Hz
78 min	15, 17, 30, 33	0.38	$\Delta P^{\text{T}} = 1.90$ $\Delta P^{\text{S}} = 0.95$	RoCoF $= -0.95$ Hz/s $\Delta f^{\text{ndr}} = -0.51$ Hz $\Delta f^{\text{ss}} = -0.23$ Hz
Branch (19, 20) is restored at the 120$^{\text{th}}$ min				
94 min	9, 10	0.12	$\Delta P^{\text{T}} = 0.60$ $\Delta P^{\text{S}} = 0.30$	RoCoF $= -0.30$ Hz/s $\Delta f^{\text{ndr}} = -0.16$ Hz $\Delta f^{\text{ss}} = -0.07$ Hz
Branch (27, 28) is restored at the 109$^{\text{th}}$ min				
109 min	27, 28	0.12	$\Delta P^{\text{T}} = 0.60$ $\Delta P^{\text{S}} = 0.30$	RoCoF $= -0.30$ Hz/s $\Delta f^{\text{ndr}} = -0.16$ Hz $\Delta f^{\text{ss}} = -0.07$ Hz
Branch (19, 20) is restored at the 120$^{\text{th}}$ min				
120 min	19, 20	0.18	$\Delta P^{\text{T}} = 0.90$ $\Delta P^{\text{S}} = 0.45$	RoCoF $= -0.45$ Hz/s $\Delta f^{\text{ndr}} = -0.24$ Hz $\Delta f^{\text{ss}} = -0.11$ Hz

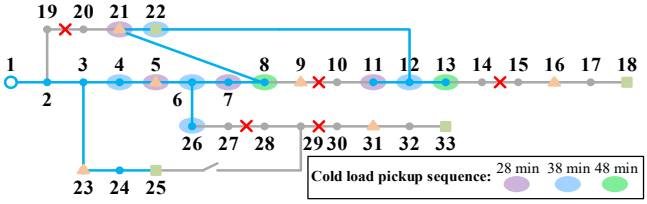

Fig. 9 Cold load pickup after faulted branch (4, 5) is restored (28-48 min).

The frequency dynamics of the first 3 load pickups (28, 38, and 48 min) are depicted in Fig. 10, using the MATLAB Simulink toolbox. The requirements for transient frequency are satisfactorily met, i.e., $|\text{RoCoF}| \leq 1$ Hz/s, $f^{\text{ndr}} \geq 49.3$ Hz,

and $f^{ss} \geq 49.5$ Hz for all cold load pickups. The secondary frequency control is triggered to restore the system frequency to 50 Hz, which is depicted in the zoom area of Fig. 10. For limited space, the frequency dynamics after 48 min are not shown, as they are similar to the first 3 cold load pickups.

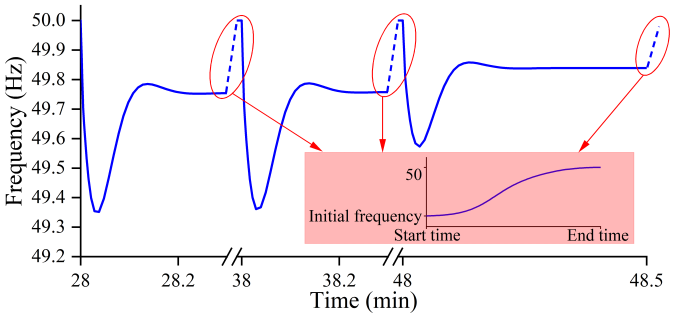

Fig. 10 Frequency dynamics of the first 3 clod load pickups (28-48 min).

B. Real-World 136-node Test Feeder

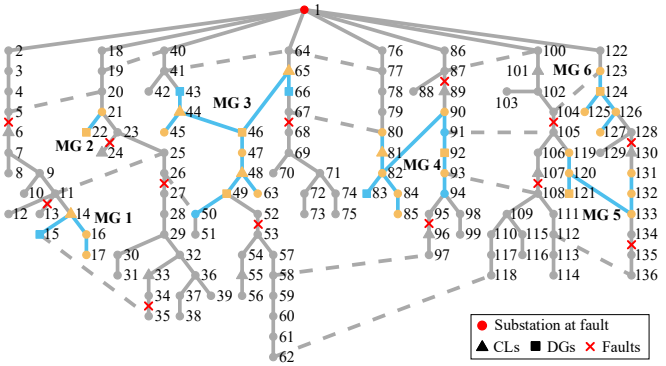

(a) The initial fault conditions

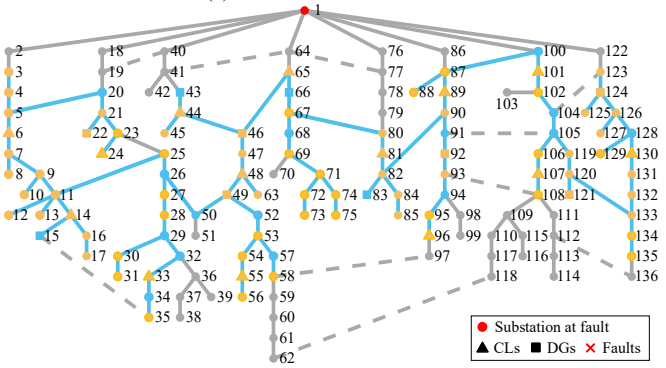

(b) The final MG topology provided by MG formation model [36]

Fig. 11 The modified real-world 136-node test feeder.

TABLE V Repair crew dispatch scheme for the faulted 136-node test feeder

Restoration time instant (min)	Faulted branches	Repair crew	Restoration time instant (min)	Faulted branches	Repair Crew
26	(87, 89)	2	38	(5, 6)	3
46	(128, 130)	1	54	(104, 105)	2
65	(23, 24)	3	78	(107, 108)	1
83	(52, 53)	2	98	(67, 68)	3
109	(26, 27)	2	117	(95, 96)	1
133	(11, 13)	3	149	(134, 135)	2
154	(34, 35)	1			

The initial condition of the 136-node system is shown in Fig. 11(a). The loss of substation and 13 permanent branch faults separate the system into 6 MGs (blue color). The energized loads are marked in yellow color. Subject to the loss of the substation, the ADN is partially energized even after all faults are cleared, and the final network is shown in Fig. 11(b) using the model [36].

There are 3 repair crews, and their dispatch scheme is detailed in TABLE V. It is indicated to restore at priority the faulted branches adjacent to CLs, e.g., (87, 89), (5, 6), and (128, 130), while the faulted branches located near the end of the system, e.g., (11, 13), (34, 35), and (134, 135), should be restored at a later stage.

This extreme case focuses on the MG interconnection and CLPU in low-inertia systems. With the help of *Phasor Measurement Units* (PMUs) and advanced control algorithms, MG interconnection is allowed [39]. If not, the 6 MGs can be treated individually, similar to the first case. It is assumed that DGs at nodes 15, 22, 46, 83, 121, and 124 are VSM-controlled ($\mathcal{V} = [15, 22, 46, 83, 121, 124]$) and the other DGs are droop-controlled ($\mathcal{D} = [43, 49, 66, 92]$).

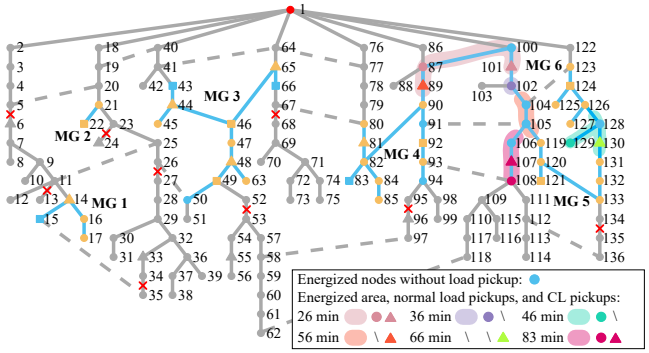

Fig. 12 The cold load pickups related to MGs 4, 5, and 6 (26-86 min).

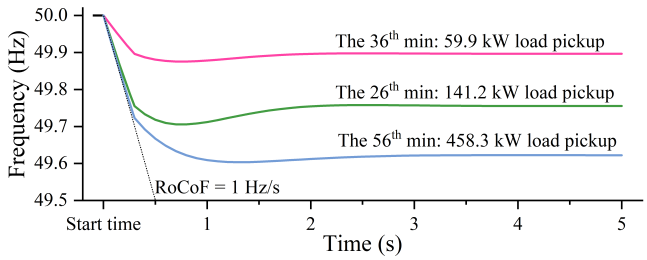

Fig. 13 Frequency drops of 3 cold load pickups at the 26th, 36th, and 56th min.

As an example, the cold load pickups during 26-86 min in MGs 4, 5, and 6 are shown in Fig. 12. At the 26th min, branch (87, 89) is restored and energized, enabling the CLs at node 101 and normal loads at node 87 to be picked up. When the frequency is restored 10 mins later at the 36th min, the loads at node 102 are picked up. Although the loads at nodes 88 and 89 could be energized by MG 4, it is unsafe to restore them due to the low inertia of MG 4. So no loads are restored in MG 4 at the 46th min. At the same time, branch (128, 130) is restored. Then MG 5 and MG 6 are interconnected, and the loads at node 129 are picked up. Later at the 56th min after branch (104, 105) is fixed, MG 4 is connected to the interconnected MG 5 and MG 6 through the path 102-104-105-119. At this time, the CLs at node 89 are picked up in the interconnected system with inertia provision from DGs 83, 121, and 124. Subsequently, the CLs at node 130 are restored at the 66th min. The large loads at node

99 are still not allowed to be energized, so no loads are picked up at the 76th min. At the 83rd min when a new branch (107, 108) is in service, the loads at nodes 107 and 108 are picked up. The following load pickups are similar. The frequency dynamics of 3 cold load pickups at the 26th, 36th, and 56th min are depicted in Fig. 13. It indicates that the primary factor limiting the amount of cold load pickup in MGs is the RoCoF, which can easily violate the preset limit due to low inertia. This underlines that cold load pickup in low-inertia MGs should be conducted carefully to avoid drastic frequency drops. In addition, it is safer to restore large loads after interconnecting more MGs. For example, picking up 458.3 kW loads is allowed at the 56th min when MG 4, MG 5, and MG 6 are interconnected. In contrast, the allowable load pickup amount before the interconnection is only 141.2 kW.

C. Comparison of Computational Complexity

TABLE VI Comparisons of computation time

Test feeders	Proposed models		Benchmark RCD model [3]*	Existing event-driven RCD model [15]*
	Event-driven RCD	SCLP		
IEEE 33-node	Max. 9.04 s Avg. 3.35 s Min. 0.03 s	Max. 0.019 s Avg. 0.007 s Min. 0.003 s	638.72 s	1212.63 s
Real-world 136-node	Max. 328.05 s Avg. 55.99 s Min. 0.24 s	Max. 0.025 s Avg. 0.012 s Min. 0.007 s	4039.48 s	> 200 min

* The computation time are obtained by solving the model without pre-assigning repair tasks to depots

The computation time of the proposed models is compared with a benchmark RCD model [3] and an existing event-driven RCD model [15] in TABLE VI. The optimality gap is set as 1% and 5% for the IEEE 33-node and real-world 136-node test feeders, respectively. It should be noted that the complexity of the proposed RCD and SCLP model reduces, as the number of remaining faults decreases in the solving process. This is illustrated by the minimum, maximum, and average computation time in TABLE VI. The computation time of the proposed SCLP model is negligible, taking advantage of the linear frequency constraints that can be easily solved. Furthermore, the proposed RCD model exhibits high tractability, with an average solution time of less than 10 s for the IEEE 33-node test feeder and 1 min for the real-world 136-node test feeder. In contrast, the benchmark RCD model [3] requires computation time exceeding 10 min and 67 min for these two test feeders. The existing event-driven RCD model [15], which introduces multiplied binary variables, further exacerbates computational complexity, requiring more than 20 min for the 33-node test feeder and becoming intractable for the 136-node test feeder. Considering the most complex case in the proposed RCD model, the computation time is maintained under 6.5 min, resulting in a reduction of 91.9% compared to the RCD model [3]. Therefore, owning to the integration of the MPC technique, the computational complexity of the proposed event-driven RCD model is significantly reduced compared to existing models, such as [3] and [15].

VII. Conclusion

By coordinating the repair crew dispatch and cold load pickup, this paper provides a dynamic restoration strategy for ADNs. Modeling repair crew dispatch using MPC allows the incorporation of stochastic repair time. Picking up cold loads in low-inertia ADNs, especially after the loss of substation, should be operated carefully to avoid frequency instability. Simulation results of the frequency-constrained SCLP model indicate that the primary factor limiting the CLPU demand is the high value of RoCoF. Potential advances of the proposed model include detailed modeling of the stochastic repair time, incorporating real-time measurement data, and improving the CLPU model.

VIII. References

[1] J. Lei, S. Gao, J. Shi, X. Wei, M. Dong, W. Wang and Z. Han, "A reinforcement learning approach for defending against multiscenario load redistribution attacks," *IEEE Trans. Smart Grid*, vol. 13, no. 5, pp. 3711-3722, Sept. 2022.

[2] C. Chen, J. Wang and D. Ton, "Modernizing distribution system restoration to achieve grid resiliency against extreme weather events: An integrated solution," *Proc. IEEE*, vol. 105, no. 7, pp. 1267-1288, July 2017.

[3] A. Arif, Z. Wang, J. Wang and C. Chen, "Power distribution system outage management with co-optimization of repairs, reconfiguration, and DG dispatch," *IEEE Trans. Smart Grid*, vol. 9, no. 5, pp. 4109-4118, Sept. 2018.

[4] B. Chen, Z. Ye, C. Chen, J. Wang, T. Ding and Z. Bie, "Toward a synthetic model for distribution system restoration and crew dispatch," *IEEE Trans. Power Syst*., vol. 34, no. 3, pp. 2228-2239, May 2019.

[5] G. Zhang, F. Zhang, X. Zhang, K. Meng and Z. Y. Dong, "Sequential disaster recovery model for distribution systems with co-optimization of maintenance and restoration crew dispatch," *IEEE Trans. Smart Grid*, vol. 11, no. 6, pp. 4700-4713, Nov. 2020.

[6] C. Wang, M. Yan, K. Pang, F. Wen and F. Teng, "Cyber-physical interdependent restoration scheduling for active distribution network via ad hoc wireless communication," *IEEE Trans. Smart Grid*, Early access, 2023. doi: 10.1109/TSG.2023.3244785.

[7] S. Lei, C. Chen, Y. Li and Y. Hou, "Resilient disaster recovery logistics of distribution systems: co-optimize service restoration with repair crew and mobile power source dispatch," *IEEE Trans. Smart Grid*, vol. 10, no. 6, pp. 6187-6202, Nov. 2019.

[8] D. Qiu, Y. Wang, T. Zhang, M. Sun and G. Strbac, "Hierarchical multi-agent reinforcement learning for repair crews dispatch control towards multi-energy microgrid resilience," *Appl. Energy*, vol. 336, April 2023. Art. no. 120826.

[9] Z. Li, W. Tang, X. Lian, X. Chen, W. Zhang and T. Qian, "A resilience-oriented two-stage recovery method for power distribution system considering transportation network," *Int. J. Electr. Power Energy Syst.*, vol. 135, Feb. 2022. Art. no. 107497.

[10] Q. Zhang, Z. Wang, S. Ma and A. Arif, "Stochastic pre-event preparation for enhancing resilience of distribution systems," *Renew. Sustain. Energy Rev.*, vol. 152, Dec. 2021. Art. no. 111636.

[11] Y. Tan, F. Qiu, A. K. Das, D. S. Kirschen, P. Arabshahi and J. Wang, "Scheduling post-disaster repairs in electricity distribution networks," *IEEE Trans. Power Syst.*, vol. 34, no. 4, pp. 2611-2621, July 2019.

[12] Q. Shi, F. Li, J. Dong, M. Olama, X. Wang, C. Winstead and T. Kuruganti, "Co-optimization of repairs and dynamic network reconfiguration for improved distribution system resilience," *Appl. Energy*, vol. 318, July 2022. Art. no. 119245.

[13] A. Arif, S. Ma, Z. Wang, J. Wang, S. M. Ryan and C. Chen, "Optimizing service restoration in distribution systems with uncertain repair time and demand," *IEEE Trans. Power Syst.*, vol. 33, no. 6, pp. 6828-6838, Nov. 2018.

[14] J. Li, M. E. Khodayar and M. R. Feizi, "Hybrid modeling based co-optimization of crew dispatch and distribution system restoration considering multiple uncertainties," *IEEE Syst. J.,* vol. 16, no. 1, pp. 1278-1288, March 2022.

[15] X. Sun, J. Chen, H. Zhao, W. Zhang and Y. Zhang, "Sequential disaster recovery strategy for resilient distribution network based on cyber–physical collaborative optimization," *IEEE Trans. Smart Grid*, vol. 14, no. 2, pp. 1173-1187, March 2023.

[16] F. Friend, "Cold load pickup issues," in *62nd Annu. Conf. Prot. Relay Eng.*, College Station, TX, USA, 2009, pp. 176-187.

[17] A. Golshani, W. Sun, Q. Zhou, Q. P. Zheng and J. Tong, "Two-stage adaptive restoration decision support system for a self-healing power grid," *IEEE Trans. Ind. Inf.*, vol. 13, no. 6, pp. 2802-2812, Dec. 2017.
[18] B. Chen, C. Chen, J. Wang and K. L. Butler-Purry, "Multi-time step service restoration for advanced distribution systems and microgrids," *IEEE Trans. Smart Grid*, vol. 9, no. 6, pp. 6793-6805, Nov. 2018.
[19] K. P. Schneider, E. Sortomme, S. S. Venkata, M. T. Miller and L. Ponder, "Evaluating the magnitude and duration of cold load pick-up on residential distribution using multi-state load models," *IEEE Trans. Power Syst.*, vol. 31, no. 5, pp. 3765-3774, Sept. 2016.
[20] Q. Zhang, Z. Ma, Y. Zhu and Z. Wang, "A two-level simulation-assisted sequential distribution system restoration model with frequency dynamics constraints," *IEEE Trans. Smart Grid*, vol. 12, no. 5, pp. 3835-3846, Sept. 2021.
[21] U. Markovic, Z. Chu, P. Aristidou and G. Hug, "LQR-based adaptive virtual synchronous machine for power systems with high inverter penetration," *IEEE Trans. Sustainable Energy*, vol. 10, no. 3, pp. 1501-1512, July 2019.
[22] D. T. Lagos and N. D. Hatziargyriou, "Data-driven frequency dynamic unit commitment for island systems with high RES penetration," *IEEE Trans. Power Syst.*, vol. 36, no. 5, pp. 4699-4711, Sept. 2021.
[23] M. Farrokhabadi et al., "Microgrid stability definitions, analysis, and examples," *IEEE Trans. Power Syst.*, vol. 35, no. 1, pp. 13-29, Jan. 2020.
[24] B. Xu, C. Wang, F. Wen, I. Palu and K. Pang. "Fault diagnosis and identification of malfunctioning protection devices in a power system via time series similarity matching," *Energy Convers. Econ.*, vol. 1, no. 2, pp. 81-92, Oct. 2020.
[25] C. Wang, K. Pang, M. Shahidehpour and F. Wen, "MILP-based fault diagnosis model in active power distribution networks," *IEEE Trans. Smart Grid*, vol. 12, no. 5, pp. 3847-3857, Sept. 2021.
[26] E. Zountouridou, G. Kiokes, A. Dimeas and N. Hatziargyriou, "A guide to unmanned aerial vehicles performance analysis–the MQ-9 unmanned air vehicle case study," *J. Eng.*, vol. 2023, no. 6, pp. 1-15, June 2023.
[27] K. Pang, C. Wang, N. D. Hatziargyriou and F. Wen, "Microgrid formation and real-time scheduling of active distribution networks considering source-load stochasticity," *IEEE Trans. Power Syst.*, Early access, 2023. doi: 10.1109/TPWRS.2023.3276008.
[28] C. Wang, K. Pang, M. Shahidehpour, F. Wen, H. Ren and Z. Liu, "Flexible joint planning of sectionalizing switches and tie lines among distribution feeders," *IEEE Trans. Power Syst.*, vol. 37, no. 2, pp. 1577-1590, Mar. 2022.
[29] M. E. Baran and F. F. Wu, "Network reconfiguration in distribution systems for loss reduction and load balancing," *IEEE Trans. Power Delivery*, vol. 4, no. 2, pp. 1401-1407, April 1989.
[30] J. Burkardt. (2014). *The Truncated Normal Distribution*. [Online]. Available: https://people.sc.fsu.edu/~jburkardt/presentations/truncated_normal.pdf
[31] F. H. Aghdam, N. T. Kalantari, B. Mohammadi-Ivatloo, "A stochastic optimal scheduling of multi-microgrid systems considering emissions: A chance constrained model," *J. Cleaner Prod.*, vol. 275, pp. 122965, Dec. 2020.
[32] S. Kancherla and I. Dobson, "Heavy-tailed transmission line restoration times observed in utility data," *IEEE Trans. Power Syst.*, vol. 33, no. 1, pp. 1145-1147, Jan. 2018.
[33] K. Pang, C. Wang, F. Wen, I. Palu, C. Feng, Z. Yang, M. Chen, H. Zhao and H. Shang, "Two-stage self-healing restoration strategy considering operating performance," *J. Energy Eng.*, vol. 146, no. 4, June 2020.
[34] Q. Zhang, K. Dehghanpour, Z. Wang, F. Qiu and D. Zhao, "Multi-agent safe policy learning for power management of networked microgrids," *IEEE Trans. Smart Grid*, vol. 12, no. 2, pp. 1048-1062, March 2021.
[35] P. Kundur, "Control of active power and reactive power," in *Power System Stability and Control*. New York: McGraw-Hill, 1994, pp. 581-695.
[36] K. Pang, C. Wang, N. D. Hatziargyriou, F. Wen and Y. Xue, "Formulation of radiality constraints for optimal microgrid formation," *IEEE Trans. Power Syst.*, early access. doi: 10.1109/TPWRS.2022.3221048.
[37] C. Wang, K. Pang, M. Shahidehpour, F. Wen and S. Duan, "Two-stage robust design of resilient active distribution networks considering random tie line outages and outage propagation," *IEEE Trans. Smart Grid*, vol. 14, no. 4, pp. 2630-2644, July 2023.
[38] K. Balu and V. Mukherjee, "Optimal siting and sizing of distributed generation in radial distribution system using a novel student psychology-based optimization algorithm," *Neural. Comput. Appl.*, vol. 33, pp. 15639–15667, June 2021.
[39] S. Sivaranjani, E. Agarwal, V. Gupta, P. Antsaklis and L. Xie, "Distributed mixed voltage angle and frequency droop control of microgrid interconnections with loss of distribution-PMU measurements," *IEEE Open Access J. Power Energy*, vol. 8, pp. 45-56, 2021.

Kaiyuan Pang received the B.E. degree in electrical engineering from Wuhan University, Wuhan, China, in 2018. He is currently working toward the Ph.D. degree in electrical engineering with Zhejiang University, Hangzhou, China. He was a visiting Ph.D. student with the School of Electrical and Computer Engineering, National Technical University of Athens, Athens, Greece, from 2021 to 2023. His research interest lies in power distribution system resilience enhancement.

Chongyu Wang received the B.E. degree from Xi'an Jiaotong University, Xi'an, China, in 2017, and the Ph.D. degree from Zhejiang University, Hangzhou, China, in 2022, both in electrical engineering. He is currently a Postdoctoral Fellow with the Department of Electrical Engineering, The Hong Kong Polytechnic University, Hong Kong SAR. He was a joint PhD student with the Department of Electrical and Electronic Engineering, Imperial College London, U.K. from 2021 to 2022. His main research interests involve resilient power systems and cyber-physical energy systems.

Nikos D. Hatziargyriou (Life Fellow, IEEE) received the Diploma degree in electrical and mechanical engineering from the National Technical University of Athens, Athens, Greece, in 1976, and the M.Sc. and Ph.D. degrees in electrical power engineering from the University of Manchester Institute of Science and Technology, Manchester, U.K., in 1979 and 1982, respectively. He is since 1984 with the Electrical and Computer Engineering School, National Technical University of Athens (NTUA), Professor in Power Systems since 1995, and Professor Emeritus since 2022. He is also part-time Professor at the University of Vaasa, Finland. He has over 10 years of industrial experience as Chairman and the CEO of the Hellenic Distribution Network Operator (HEDNO) (2015-2019) and as Executive Vice-Chair and Deputy CEO of the Public Power Corporation (PPC) (2007-2012), responsible for the Transmission and Distribution and the Islands Divisions. He is author of 300 journal publications and 600 conference proceedings papers. He is included in the 2016, 2017, and 2019, Thomson Reuters lists of the top 1% most cited researchers. He is 2020 Globe Energy Prize laureate, recipient of the 2017 IEEE/PES Prabha S. Kundur Award and the 2023 IEEE Herman Halperin Electric Transmission and Distribution Award. He was Chair of the Power System Dynamic Performance Committee of IEEE, EiC of the IEEE TPWRS, and is currently EiC-at-Large for IEEE PES Transactions. He is honorary member of CIGRE and was the Chair of CIGRE SC C6 "Distribution Systems and Distributed Generation." He was the Chair and Vice-Chair of the EU Technology and Innovation Platform on Smart Networks for Energy Transition (ETIP SNET). He has participated in more than 60 R&D projects funded by the EU Commission, electric utilities and industry for fundamental research and practical applications.

Fushuan Wen (Fellow, IEEE) received the B.E. and M.E. degrees from Tianjin University, Tianjin, China, in 1985 and 1988, respectively, and the Ph.D. degree from Zhejiang University, Hangzhou, China, in 1991, all in electrical engineering. He joined Zhejiang University as a Faculty Member in the School of Electrical Engineering in 1991, where he has been a Full Professor since 1997; he has also been a Full Professor with the Hainan Institute, Zhejiang University since 2022. He is a part-time distinguished professor in Hangzhou Dianzi University, China, and a visiting principal research scientist in Shenzhen Institute of Artificial Intelligence and Robotics for Society,

China. He has been listed in "Most Cited Chinese Researchers" in seven consecutive years since 2015 by Elsevier. He is the *Editor-in-Chief of Energy Conversion and Economics* (IET), the deputy Editor-in-Chief of *Automation of Electric Power Systems*, and serves as the editor, subject editor and associate editor of several international journals. His research interests include power industry restructuring, power system alarm processing, fault diagnosis and restoration strategies, smart grids and electric vehicles, as well as artificial intelligence applications in power and integrated energy systems.